Magnetic Resonance Imaging 57 (2019) 83–94

Contents lists available at ScienceDirect

Magnetic Resonance Imaging

journal homepage: www.elsevier.com/locate/mri

Technical report

A stereotaxic MRI template set of mouse brain with fine sub-anatomical delineations: Application to MEMRI studies of 5XFAD mice

Binbin Nie[a,b,g,1], Di Wu[c,1], Shengxiang Liang[a,b,d,e,1], Hua Liu[a,b], Xi Sun[a,b,e], Panlong Li[a,b,e], Qi Huang[a,b], Tianhao Zhang[a,b], Ting Feng[a,b,e], Songtao Ye[f], Zhijun Zhang[c,*], Baoci Shan[a,b,g,**]

[a] Beijing Engineering Research Center of Radiographic Techniques and Equipment, Institute of High Energy Physics, Chinese Academy of Sciences, Beijing 100049, China
[b] School of Nuclear Science and Technology, University of Chinese Academy of Sciences, Beijing 100049, China
[c] Department of Neurology, Affiliated ZhongDa Hospital, Neuropsychiatric Institute, School of Medicine, Southeast University, Nanjing 210009, China
[d] College of Rehabilitation Medicine, Fujian University of Traditional Chinese Medicine, Fuzhou 350122, China
[e] Physical Science and Technology College, Zhengzhou University, Zhengzhou 450001, China
[f] College of Information Engineering, Xiangtan University, Xiangtan 411105, China
[g] CAS Center for Excellence in Brain Science and Intelligence Technology, Shanghai 200031, China

ARTICLE INFO

Keywords:
MEMRI
Mouse brain
Brain atlas
Stereotaxic template
5XFAD

ABSTRACT

Purpose: Manganese-enhanced magnetic resonance imaging (MEMRI) can help us trace the active neurons and neuronal pathway in transgenic mouse AD model. 5XFAD has been widespread accepted as a valuable model system for studying brain dysfunction progresses in the courses of AD. To further understand the development of AD at early stages, an effective and objective data analysis platform for MEMRI studies should be constructed.
Materials and methods: A set of stereotaxic templates of mouse brain in Paxinos and Franklin space, "the Institute of High Energy Physics Mouse Template", or IMT for short, was constructed by iteratively registration and averaging. An atlas image was reconstructed from the Paxinos and Franklin atlas figures and each sub-anatomical segmentation was assigning a unique integer. An analysis SPM plug-in toolbox was further created, that automates and standardizes the time-consuming processes of brain extraction, tissue segmentation, and statistical analysis for MEMRI scans.
Results: The IMT comprised a T2WI template image, a MEMRI template image, intracranial tissue segmentations, and accompany with a digital mouse brain atlas image, in which 707 sub-anatomical brain regions are delineated. Data analyses were performed on groups of developing 5XFAD mice to demonstrate the usage of IMT, and the results shows that abnormal neuronal activity occurs at early stage in 5XFAD mice.
Conclusion: We have constructed a stereotaxic template set of mouse brain named IMT with fine delineations of sub-anatomical structures, which is compatible with SPM. It will give a widely range of researchers a standardized coordinate system for localization of any mouse brain related data.

1. Introduction

Neuronal activity dysfunction is an important indicator of Alzheimer's disease (AD) at early stages, which appears prior to cognitive impairment [1]. Manganese-enhanced magnetic resonance imaging (MEMRI) is a noninvasive in vivo imaging technique that is widely used for these neuronal activity detecting [2]. With the assistance of manganese ions (Mn^{2+}), the MEMRI can help us trace the active neurons and neuronal pathway [3]. Transgenic mouse AD model, such as 5XFAD, has been widely accepted as a valuable model system for studying such dysfunction progresses in the courses of AD [4,5]. Our previous study has performed longitudinal MEMRI in developing 5XFAD mice [6]. By manually tracing out 12 regions of interest (ROIs), we have found that the basal neuronal activity is aberrant increased at early stage of AD [6]. Given the critical role of developing 5XFAD mice in AD, an efficient data analytic method is necessary, which could facilitate better understanding of AD developments benefits from rodents.

Similar with other modalities of magnetic resonance imaging (MRI), MEMRI images could be analyzed automatically and objectively by either voxel-wise or ROI-wise (region of interest) methods, after they

* Corresponding author.
** Correspondence to: B. Shan, Institute of High Energy Physics, Chinese Academy of Sciences, Beijing 100049, China.
E-mail addresses: janemengzhang@vip.163.com (Z. Zhang), shanbc@ihep.ac.cn (B. Shan).
[1] These three authors contribute equally to this article.

https://doi.org/10.1016/j.mri.2018.10.014
Received 28 June 2018; Received in revised form 16 October 2018; Accepted 18 October 2018

are spatially standardized into a common space according to a predefined template image. In the past decades, several MRI templates have been constructed for mouse brain [7–10]. In terms of MEMRI studies, a set of templates of developing neonatal mouse brain have been created, comprising stages of brain development between postnatal day 1 (P1) to P11 [11]. It is of great value and has facilitated the early postnatal studies by MEMRI techniques, despite its limitations in late infancy researches and poor sub-anatomical segmentations. Therefore, in view of the MEMRI imaging of late infancy is also playing an important role in developing studies, it is also imperative to construct an adult MEMRI template.

A mouse brain template alone is incomplete without an atlas system offering stereotaxic anatomical information. In the data analysis by either voxel-wise or ROI-wise, accurate and subtle sub-anatomical segmentations would improve the reproducibility and consistency. Recently, several mouse brain atlases, in which dozens of anatomical regions are delineated, have been constructed based on multi-modality neuroimaging studies [8,11,12]. To distinguish more sophisticated sub-anatomical regions, conventional two-dimensional histochromic atlases are constructed, such as the Allen brain atlas [13,14] and the Paxinos and Franklin mouse brain atlas [15]. There are hundreds of sub-anatomical structures delineated in histochromic atlases. To applicate it in MEMRI studies, these histochromic slices, however, should be upgraded from two-dimensional to three-dimensional and further co-registered with the mouse brain template.

Motivated by further understanding the development of AD at early stages, our work focused on establishing an effective and objective data analysis platform for MEMRI studies. To do so, a set of stereotaxic templates of mouse brain in Paxinos and Franklin space was constructed, which we call the Institute of High Energy Physics Mouse Template – or IMT for short. This constructed IMT comprised a T2-wighted (T2WI) template image, a set of tissue probability maps (TPM), and a MEMRI template image. The IMT is compatible with one of the most popular neuroimaging data analysis software – the statistical parametric mapping (SPM), so that voxel-wise analysis of mouse brain could be performed simply in SPM [16]. Moreover, a digital atlas image of mouse brain was also constructed accompanied with the IMT, in which 707 sub-anatomical structures were delineated. This atlas image could be served as an optimal choice for subtle phenotypic analyses of developing 5XFAD mice. Finally, voxel-wise analysis was performed on the MEMRI images of developing 5XFAD mice at early ages (1-, 2-, 3-, and 5-month-old respectively) to demonstrate the usage of IMT. All the significant voxels with neuronal activity dysfunction at each development stage of 5XFAD were found out, and then two significant ROIs, the hippocampus and amygdala, were extracted and further analyzed.

Our constructed IMT is compatible with the SPM. In addition, we are making the IMT and the software package openly available to the research community. This package will give a widely range of researchers (within or outside of neuroimaging) a standardized coordinate system for normalization, segmentation and localization of any mouse brain related data. This will also allow for foster collaboration across research groups and institutions. The IMT and the software package are available by contacting the corresponding author at shanbc@ihep.ac.cn.

2. Material and methods

An overview of this study is presented in Fig. 1, comprising the procedure for the IMT construction and its application to data analysis of MEMRI images.

2.1. Animals

Thirty-eight healthy male adult C57BL/6 mice (age range, 10–11 weeks old; weight range, 25–35 g) were used for the IMT construction. Twenty-three of them were used for T2WI template construction, while fifteen were used for MEMRI template creation.

Developing 5XFAD mice and its corresponding age-matched C57BL6/J wild mice were enrolled for IMT application and evaluation. 5XFAD mice were developed using the method described by Oakley et al. [17], which co-express human APP and presenilin 1 with five familial AD mutations (APP K670N/M671L + I716V + V717I and PS1 M146L + L286V). These mice were gifts from Prof. Xiaochun Chen (Department of Fujian Medical University, Fuzhou, China). Mice were generated and maintained in the C57BL/6 background. Genotyping was performed by polymerase chain reaction analysis of tail DNA. To longitudinally track neuronal activity alterations at early stage of AD, four developing stages were encompassed in this study, involving 1-, 2-, 3-, and 5-month-old. In each stage, there are six 5XFAD mice and six age-matched C57BL6/J wild mice underwent in vivo MEMRI imaging. All experiments were conducted in accordance with the National Institutes of Health Guide for the Care and Use of Laboratory Animals and were approved by Jiang Su Animal Care and Use Committee.

2.2. MRI data acquisition

During MRI scan, all mice were anesthetized using inhaled isoflurane/O2 (3% for induction and 1.5–2% for maintenance), and prostrated on a custom-made holder to minimize head motion while respiration was monitored at a rate of 50 breaths per min. All datasets were acquired on a 7.0 T animal MRI scanner (70/16 PharmaScan, Bruker Biospin GmbH, Germany) in Nanjing, using a 72 mm transmit-only RF coil and a receive-only quadrature surface coil.

For IMT construction, T2-wighted (T2WI) structural images of the twenty-three healthy adults were obtained with a RARE sequence (RARE factor = 8, TR = 17,483 ms, TE = 36 ms, matrix size $256 * 256 * 75$, voxel size $0.06 * 0.05 * 0.2$ mm, no slice gap). Then, MEMRI experiment of the other fifteen healthy adults were conducted. All these mice were injected with manganese chloride (MnCl2·4H2O, Bio Basic Inc., Canada) dissolved in bicine (di(hydroxyethyl)glycine, Sigma-Ulrich, UK) buffer pH 7.4. To reduce acute peripheral Mn^{2+} overexposure, each mouse was injected intraperitoneally in four fractionated doses of 13.95 mg/kg MnCl2·4H2O with an inter-injection interval of 24 h. Then, MEMRI images were obtained 24 h after the last injection, with a 3D-MDEFT sequence (TR = 5240 ms, TE = 5 ms, matrix size $256 * 256 * 75$, voxel size $0.06 * 0.05 * 0.2$ mm, no slice gap).

MEMRI experiment of the developing 5XFAD mice and its corresponding C57BL6/J wild mice was conducted using the similar protocols as detailed above. The MEMRI images were obtained with a RARE sequence (RARE factor = 4, TR = 1430 ms, TE = 8.89 ms, matrix size $384 * 384 * 30$, voxel size $0.06 * 0.06 * 0.5$ mm, no slice gap). Moreover, the T2WI coplanar image of each mouse was also obtained, which is similar with its corresponding MEMRI imaging.

Finally, all the Bruker original images were converted to DICOM format with programs (Paravision 5.0) in the scanner.

2.3. Construction of the IMT

The flowchart for IMT construction is shown in Fig. 2. The IMT comprised a T2WI template image (Fig. 2A), a set of TPM (Fig. 2B), and a MEMRI template image (Fig. 2C).

2.3.1. Construction of a T2WI template image in IMT

All these 23 T2WI images included in this study were inspected and found equally of high quality in terms of the image contrast, noise level and resolution. Firstly, the nonuniform image intensity caused by surface coil of all these T2WI images were corrected using N4 algorithm [18]. The T2WI structural template image was created recursively by registering [19–22] and averaging, using affine and non-linear registration algorithm in SPM (Wellcome Department of Cognitive Neurology, London, UK) (*Step 1*) [21]. The latest mean T2WI image is accepted as the final T2WI template image in IMT, until the mean

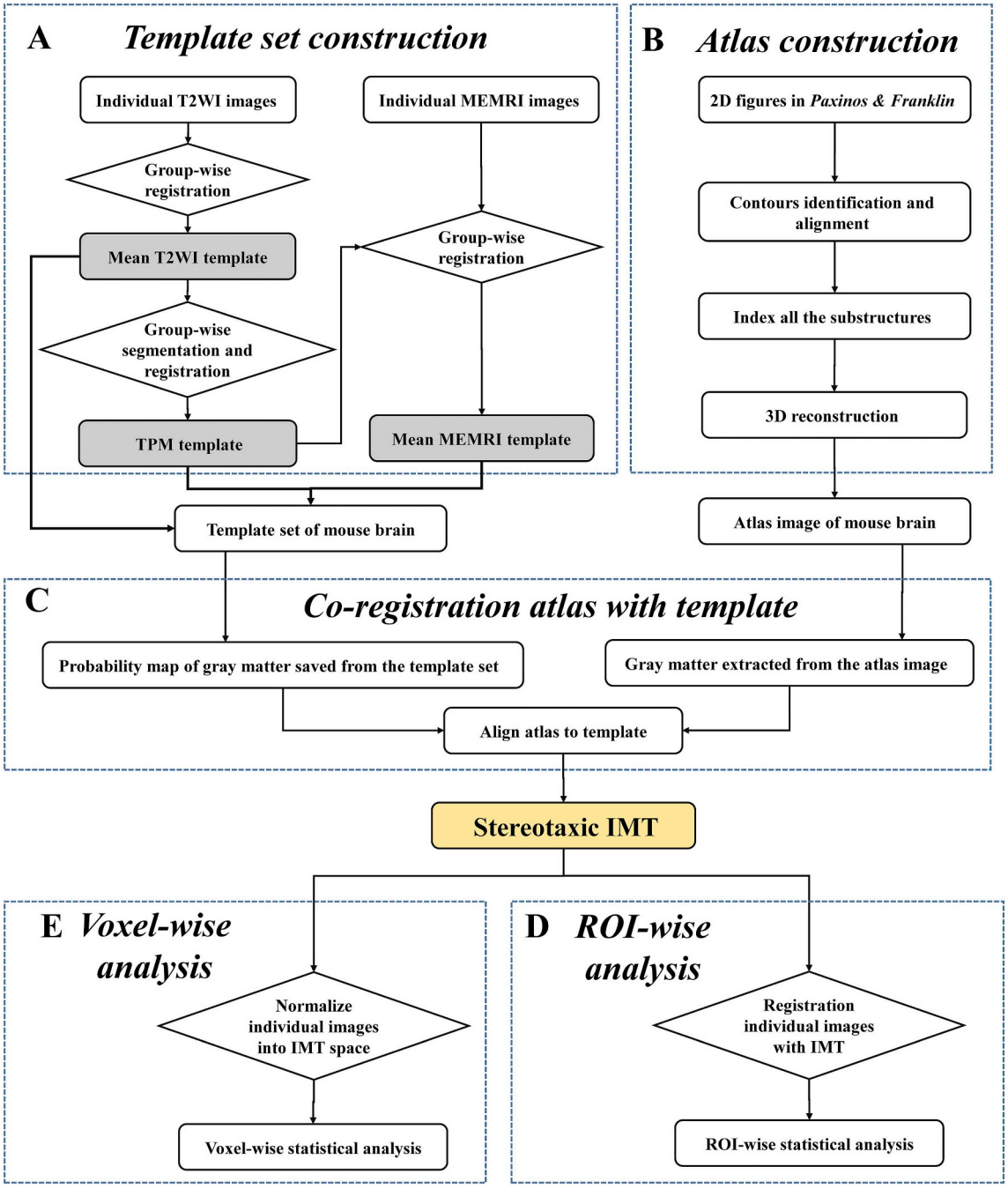

Fig. 1. Flow chart of IMT construction and its application for both ROI-wise and voxel-wise analysis.

standard residual difference (SD) between two adjacent mean T2WI images is < 5%.

2.3.2. Construction of a set of TPM in IMT

The constructed T2WI template image (Fig. 2A) was initially segmented into six types based on image intensity using FAST (FMRIB's Automated Segmentation Tool) segmentation toolbox in FSL (FMRIB Software Library) (*Step 2*), comprising not only three intracranial tissues parts such as the gray matter (*GM*), the white matter (*WM*) and the cerebrospinal fluid (*CSF*), but also three extracranial types such as skull, extracranial soft tissues and background. These initial segmentations were saved as mask images. Afterwards, the TPM of mouse brain was created recursively by segmentation, spatially registering and averaging in SPM (*Step 3*). In detail, using these initial segmentations as reference inputs, all these 23 original T2WI images were segmented and normalized using DARTEL (diffeomorphic anatomical registration through exponentiated lie) algorithm [23]. Then, these normalized tissue class maps were averaged and regularized, and then selected as a new reference. Afterwards, the original T2WI images were segmented, registered, averaged and regularized recursively, until the SD between two adjacent *GM* of mean TPM is < 5%. Finally, the latest mean TPM is accepted as the final TPM of mouse brain in IMT (Fig. 2B).

2.3.3. Construction of a MEMRI template image in IMT

All these 15 MEMRI images included in this study were inspected and were found equally of high quality in terms of the image contrast, noise level and resolution. Using the constructed TPM as a reference input, all these 15 MEMRI images were normalized into the IMT space

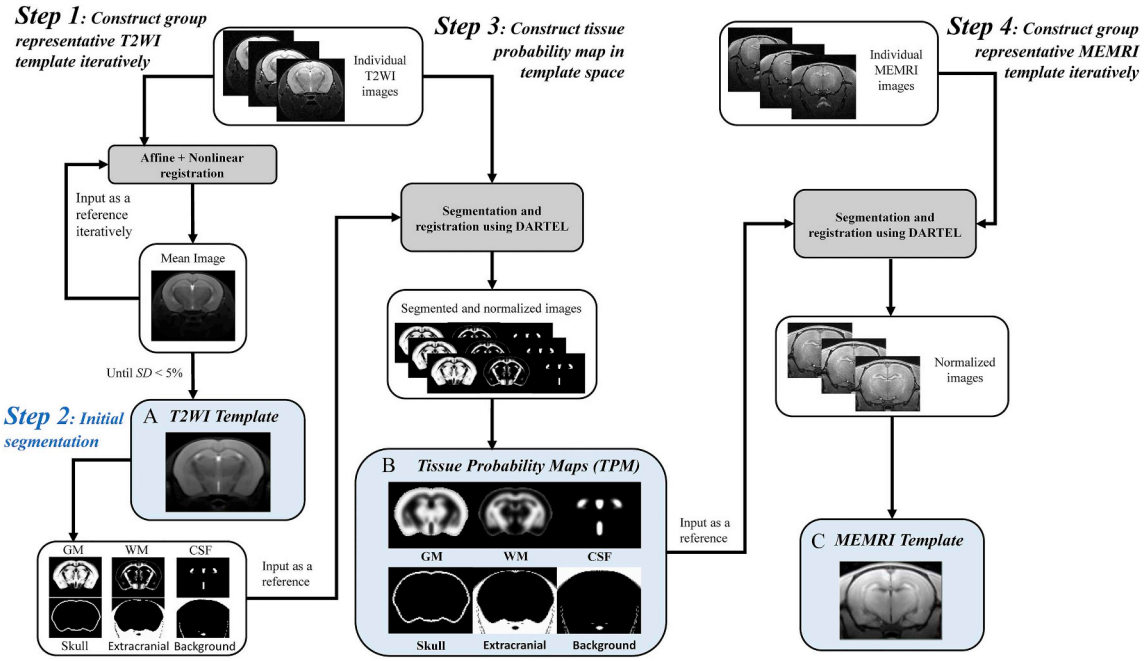

Fig. 2. Flow chart for creating population IMT of mouse brain. Step 1: Constructing T2WI structural template image recursively by registering and averaging, using affine and non-linear registration. The final structural template image is accepted until the mean standard residual difference (*SD*) between two adjacent mean images is < 5%. Step 2: Segmenting the constructed template image into six parts based on image intensity, comprising the gray matter (*GM*), the white matter (*WM*), the cerebrospinal fluid (*CSF*), skull, extracranial tissues and background. Step 3: Constructing tissue probability maps in IMT space by DARTEL (diffeomorphic anatomical registration through exponentiated lie) segmentation and registration, using the initial segmentation images as reference. Step 4: Constructing MEMRI template image recursively by DARTEL registration and averaging based on the created TPM in Step 3, until the SD between two adjacent mean images is < 5%. Our constructed IMT comprise three parts: (A) T2WI structural template image, (B) TPM, and (C) MEMRI template image.

using DARTEL algorithm in SPM (*Step 4*). These normalized MEMRI images were then averaged to create a mean MEMRI image and selected as a new reference. Then, all these 15 original MEMRI images were registered and averaged recursively using affine and nonlinear transformation, until the SD between two adjacent average MEMRI images is < 5%. The latest mean MEMRI image is accepted as the final MEMRI template (Fig. 2C).

2.4. Construction of the digital mouse brain atlas from the Paxinos and Franklin atlas

The digital mouse brain atlas image was constructed based on the 2nd edition of Paxinos and Franklin atlas [15], using the method described in [21,26]. In detail, all the 2D figures in [15], from the anterior part of cerebrum (Z_{bregma} + 3.56 mm) to the posterior part of

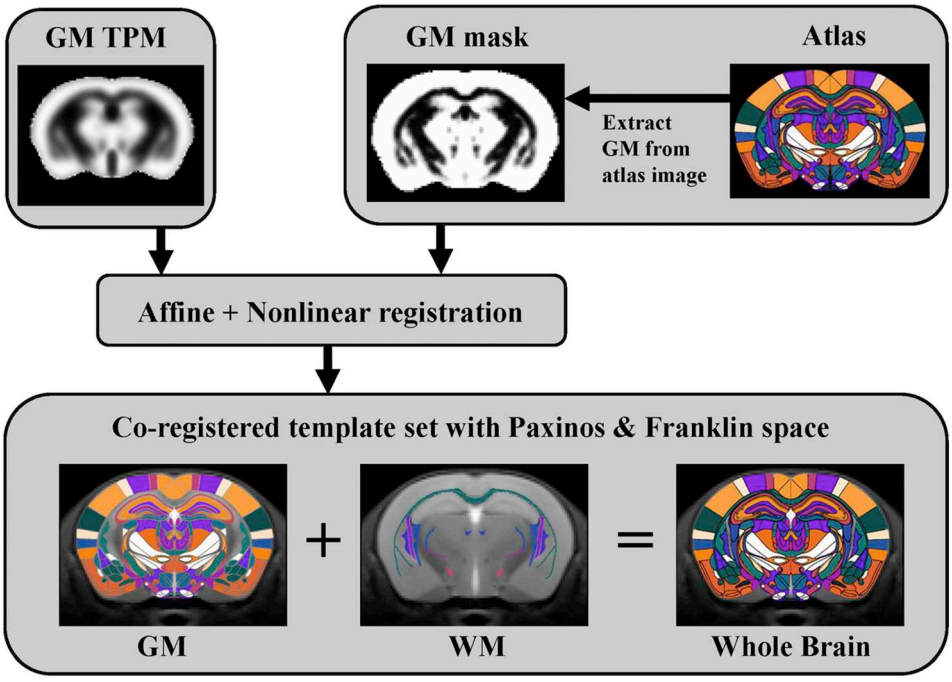

Fig. 3. Flow chart for co-registration the IMT with Paxinos & Franklin atlas space.

cerebellum ($Z_{bregma} - 8.12$ mm), were used for mouse brain atlas construction. The background of these figures, including the structure labels and coordinate grids, was removed. Then the outline and internal contours were identified and further enhanced and smoothed by image erosion and dilation [21,26]. Moreover, the slice-to-slice realignment was performed by translation to eliminate section transformation generated during specimen fixation, sectioning, and staining. Several landmarks were used in this slice-to-slice outline realignment. For example, the midline of the coronal plane was used to align the diagrams along the x-axis, while several subtle substructures such as 'IG' and 'cg' were used to align them along the y-axis. The realignment of the internal contour of each tract was also translated according to both the sagittal and transverse sections.

Each sub-anatomical structure in the atlas image was given a unique integer as an index. The laterality information was preserved by assigning odd/even integers for right/left corresponding structures. In this study, 707 sub-anatomical structures could be identified in the digital atlas. By doing so, the graphical representation of the atlas was now in the form of 3D tomographic image data, which has 97 slices with a uniform inter-slice separation of 0.12 mm. This final 3D atlas image was saved as SPM compatible NIFTI format. With this digital atlas, a sub-anatomical structure could be queried by simply reading the voxel index inside the structure.

Moreover, the stereotaxic coordinates of this mouse brain atlas were defined, where the x-axis is negative to the left from the midline and positive to the right, the y-axis is positive toward the ventral direction relative to the dorsal direction, and the z-axis is positive toward the olfactory bulb direction relative to the bregma and negative to the cerebellum direction.

2.5. Standardization of the IMT into the Paxinos and Franklin space

To standardize the template into the stereotaxic Paxinos and Franklin space, the IMT was co-registered with the constructed atlas image [21,26]. The flowchart for co-registration of the IMT to the atlas image is shown in Fig. 3. Firstly, a pseudo *GM* probability image was created from the constructed atlas image. For this purpose, all the gray matter substructures, comprising cortex and nuclei, were extracted from 707 anatomical structures and then merged. Afterwards, each voxel was randomly assigned an image intensity between 0.90 and 0.99 according to the probability value of *GM* TPM. Finally, this pseudo *GM* probability image was further smoothed using an isotropic Gaussian kernel with a full width half maximum (FWHM) of two voxels to smooth the outline and internal contours.

The pseudo *GM* probability image was chosen as the target image, and the *GM* TPM from IMT was chosen as the image to be registered and transformed. The intensity-based affine transformation algorithm and subsequent non-linear warping algorithm in SPM were employed to co-register the *GM* TPM with this target atlas image, and carried all the other template images of the IMT along [27].

This co-registered template set is the final IMT in this study. It is a stereotaxic template set in Paxinos and Franklin space and has fine sub-anatomical delineations.

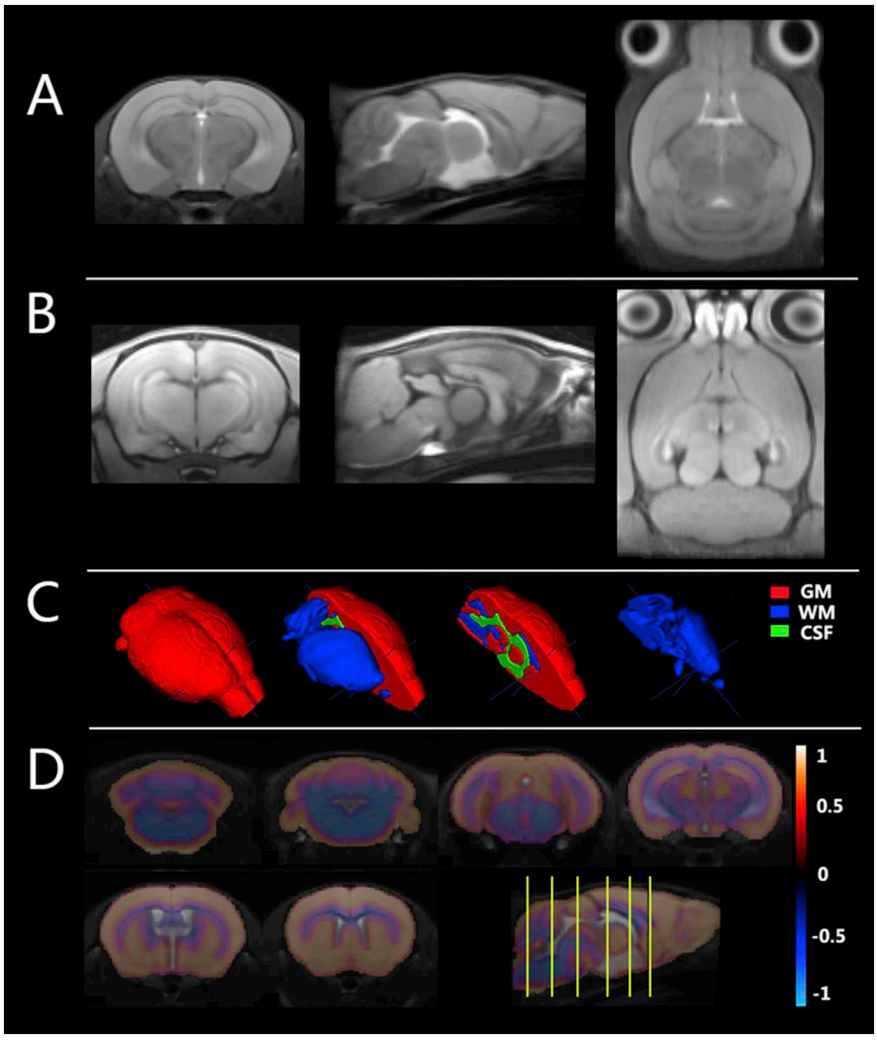

Fig. 4. The constructed IMT in Paxinos & Franklin space. (A) The axial, sagittal and coronal views of the constructed T2WI structure template. (B) The axial, sagittal and coronal views of the constructed MEMRI template. (C) The 3D rendering of the constructed tissue class map in template space. It is shown in different artificial colors and its corresponding illustration is listed to the right of (C). Three tissue classes can be identified, of which the gray matter (*GM*), the white matter (*WM*) and the cerebrospinal fluid (*CSF*) are shown in red, blue and green respectively. The cross point of dark blue dot lines represent the origin point D3V. (D) Superimposing the constructed TPM on the corresponding T2WI structure template. Six coronal slices and a sagittal view are displayed. The TPM is presented in pseudo color, in which the *GM* is displayed in warm color and the *WM* is in cool color. And its corresponding color bar stands for the probability value of each voxel and is listed to the right of panel (D). (For interpretation of the references to color in this figure legend, the reader is referred to the web version of this article.)

2.6. Data analysis of MEMRI images with the IMT

Multi-subject voxel-wise analysis and subsequent ROI-wise analysis were performed on groups of developing 5XFAD mice and its corresponding age-matched C57BL6/J wild mice to demonstrate the usage and accuracy of IMT. Briefly, the voxel size of all the MEMRI images from both groups of 1-, 2-, 3-, and 5-month-old mice were scaled up in the NIFTI header by the factor of 8 to better approximate human dimensions [21,22]. They were standardized into the IMT space via our constructed MEMRI template using affine and nonlinear transformations and then resliced to $1 \times 1 \times 1\,mm^3$ (after zooming) [21,22] in SPM12. Afterwards, these resliced images were smoothed by a Gaussian kernel with a FWHM of $2 \times 2 \times 2\,mm^3$.

These preprocessed MEMRI images were then analyzed voxel-by-voxel based on the framework of the general linear model (GLM) in SPM12. To identify signal differences between the 5XFAD mice and its corresponding age-matched C57BL6/J wild mice, two-sample *t*-test [28] was performed at each month-old stage. Proportional scaling and intensity normalization were applied to account for global confounds based on an unbiased scale factor [29]. Brain regions with significant MEMRI changes in 5XFAD mice were identified using $P < 0.001$. False discovery rate (FDR) correction ($P < 0.05$) for multiple comparisons was also conducted at the cluster level.

According to the voxel-wise analysis results, two significant ROIs, bilateral hippocampus and bilateral amygdala, were selected. The mean signal intensity of all voxels in these ROIs was further calculated. Two-tailed Student's t-test was applied to detect the differences between 5XFAD and wild-type mice. $P < 0.05$ was considered statistically significant.

3. Results

3.1. The constructed IMT and tissue segmentations

Our constructed stereotaxic IMT in Paxinos and Franklin space is shown in Fig. 4. Both the T2WI (Fig. 4A) and MEMRI template images (Fig. 4B) are shown in gray-scaled. The 3D rendering of intracranial tissue classes of TPM is shown in pseudo-color (Fig. 4C), in which the *GM*, *WM* and *CSF* are shown in red, blue and green respectively. Moreover, both *GM* and *WM* probability maps are superimposing on the T2WI template image, as shown in Fig. 4D. In order to distinguish the *WM* from the *GM* in Fig. 4D, the tissue probability map of the *WM* were transformed to negative values. As illustrated in Fig. 4, our constructed IMT set are sharing a common space.

3.2. The constructed atlas image in IMT

Coronal slices of the constructed mouse brain atlas image is shown in Fig. 5, in which the corresponding bregma coordinates is listed below each slice. As an example, one slice (Bregma −1.94 mm) is shown in Fig. 5B, in which all the distinguishable anatomical structures are labeled out by an integer as the VOI ID. Furthermore, the detailed information on all sub-anatomical structures of this slice, including the VOI ID, anatomical name and integer image intensity, are listed in Appendix 0.

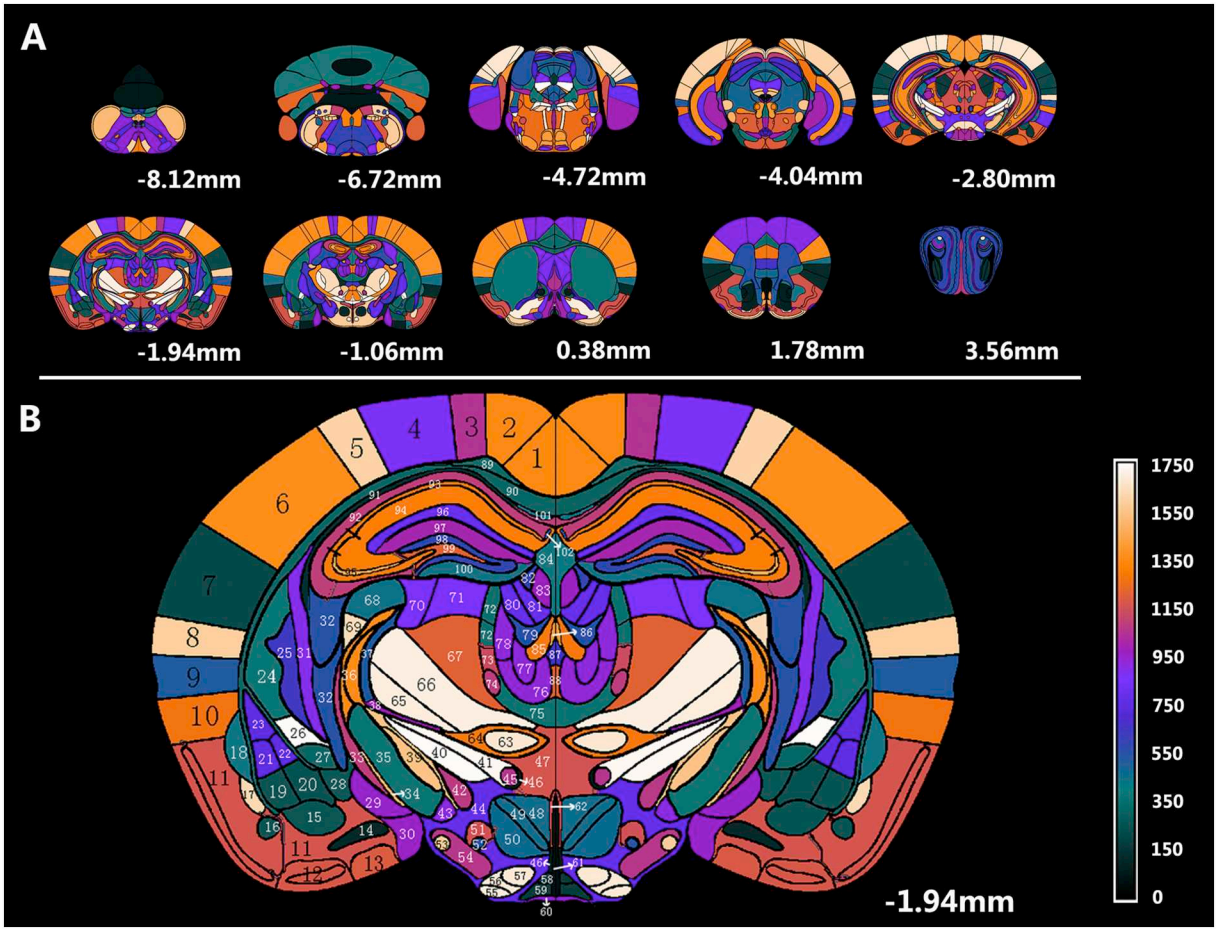

Fig. 5. The constructed atlas of mouse brain in Paxinos & Franklin space. (A) Ten coronal slices and its corresponding Z_{bregma} coordinates. (B) One randomly selected slice. All the identified anatomical structure in (B) are marked out by an integer as the VOI ID. The corresponding detailed information of each VOI ID can be found in Appendix 0. Every identified anatomical structure is displayed in pseudo color. The color bar stands for the artificial index of identified anatomical structure and is shown at the bottom to the right.

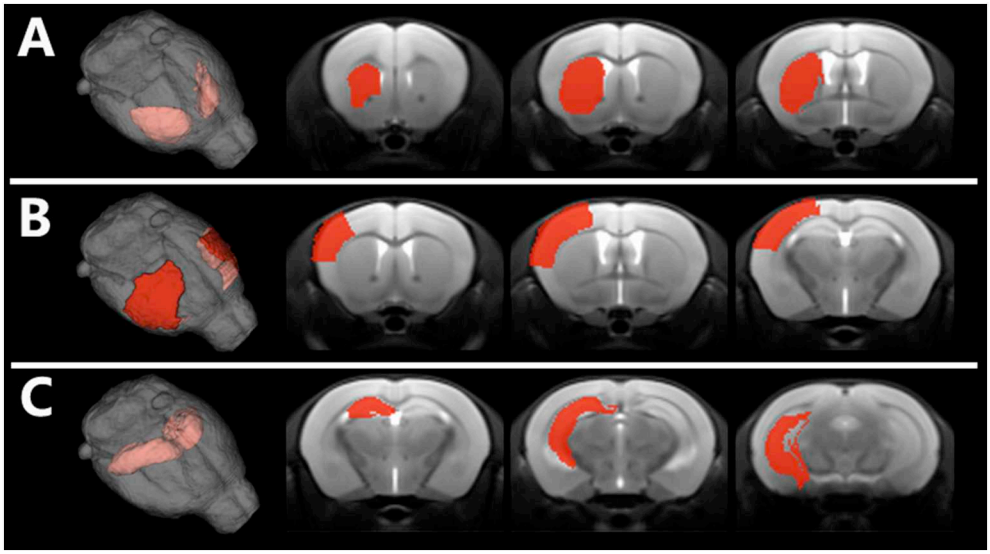

Fig. 6. Superimposing three representative anatomical structures on the IMT. The selected anatomical structures are extracted from the constructed mouse brain atlas and presented in artificial color. The co-registered mouse brain T2WI template is presented in gray-scale as a background. The three selected anatomical structures are, respectively, (A) corpus striatum, (B) somatosensory cortex, and (C) hippocampus.

Furthermore, the co-registration accuracy between the stereotaxic IMT and the atlas image is qualitatively and then quantitatively evaluated. Three representative anatomical structures, i.e., corpus striatum (CPu), somatosensory cortex, hippocampus (Hip), are selected from the mouse brain atlas image and overlaid on the T2WI template image of IMT, as shown in Fig. 6. For quantitative evaluation, an expert was invited to manually trace out the CPu and Hip from the T2WI template image separately using the ImageJ software [33], blinded to the atlas image. Three volumetric and spatial correspondence measures [21,22,26], i.e., the Dice similarity coefficient (D_{coeff}) [27] and the proportions of false-positive (*FP*) and false-negative (*FN*) results [30–32], are calculated between the manual-traced ROI ($O_{template}$) and the atlas-derived ROI (O_{atlas}), as detailed in [21,22,26]. All these quantitative evaluation results are listed in Table 1. The D_{coeff} between the IMT and atlas are > 85%, while the *FP* and *FN* are < 10%. Therefore, we could conclude that the IMT has been co-registered with the atlas image in the Paxinos and Franklin space excellently.

3.3. Estimation and application of the IMT

3.3.1. Spatially normalization of MEMRI images

Prior to statistical analysis either based on voxels or ROIs, all the individuals should be standardized into a common space according to a predefined template set. This is a crucial preprocessing step in MEMRI studies. Therefore, the spatial normalization accuracy of the developing 5XFAD MEMRI images were quantitatively evaluated. Those three volumetric and spatial correspondence measures mentioned above, comprising the D_{coeff}, the *FP* and the *FN*, are also calculated between the normalized MEMRI images and the MEMRI template image in IMT, as listed in Table 2. All the twelve mice in each stage were involved in this calculation. As illustrated, across the different developing stages of 5XFAD and healthy mice brain, the D_{coeff} between all the normalized MEMRI images and the IMT are > 95%, while both the *FN* and *FP* are < 10%. Therefore, we could conclude that all these individual MEMRI images have been normalized into the IMT space precisely.

Table 1
Volumetric and spatial correspondence measures between the mouse brain atlas image and the IMT.

	D_{coeff} (%)	*FP* (%)	*FN* (%)
Corpus striatum (CPu)	87.40	7.17	5.56
Hippocampus (Hip)	75.05	20.14	12.08

D_{coeff} (%): Dice similarity coefficient (the excellent agreement value is > 80%).
FP (%): The proportions of false-positive (the optimal value is 0%).
FN (%): The proportions of false-negative (the optimal value is 0%).

Table 2
Volumetric and spatial correspondence measures between the normalized MEMRI images and the IMT.

	1-month old	2-month old	3-month old	5-month old
D_{coeff} (%)	95.03 ± 0.48	95.90 ± 0.19	95.96 ± 0.25	95.50 ± 0.38
FP (%)	8.16 ± 0.62	6.23 ± 0.68	5.29 ± 0.40	6.51 ± 0.74
FN (%)	7.39 ± 0.51	5.73 ± 0.61	4.87 ± 0.35	5.94 ± 0.65

D_{coeff} (%): Dice similarity coefficient (the excellent agreement value is > 80%).
FP (%): The proportions of false-positive (the optimal value is 0%).
FN (%): The proportions of false-negative (the optimal value is 0%).

3.3.2. Data analysis of MEMRI images

The MEMRI images of developing 5XFAD mice were analyzed firstly voxel-by-voxel and then based on significant ROIs. The data analysis results are shown in Fig. 7 and Table 3.

Comparing with a group of age-matched wild-type mice, there are extensive brain regions showing increased signal in 1-month-old 5XFAD. The hyper-signal regions are decreased in 2-month-old 5XFAD, and gradually increased in 3- and 5-month-old stages. As shown in Fig. 7A–D, throughout all these development stages of 5XFAD, signal in the bilateral hippocampus is always significantly increased. This superficial phenomenon is also appeared in amygdala, except at the stage of 3-month-old.

Moreover, bilateral of these two significant ROIs, hippocampus and amygdala, were extracted and further analyzed. As shown in Fig. 7E–H, comparing with wild-type mice, the signal of bilateral hippocampus in 5XFAD mice is always significantly increased during the development stages, while it is increased in unilateral amygdala at 1-, 2- and 5-month-old. In addition, these extracted ROI signals could be used in correlation analysis with ethology [6].

4. Discussion

In this current study, a stereotaxic template set of mouse brain named IMT was constructed for data analysis of MEMRI images, and a group of developing 5XFAD mice were used for evaluation and application. The IMT was in the widely used Paxinos and Franklin coordinate space, together with a fine delineated digital mouse brain atlas image. Furthermore, to make it easy to use in routine data analyses, the IMT is incorporated with the SPM software.

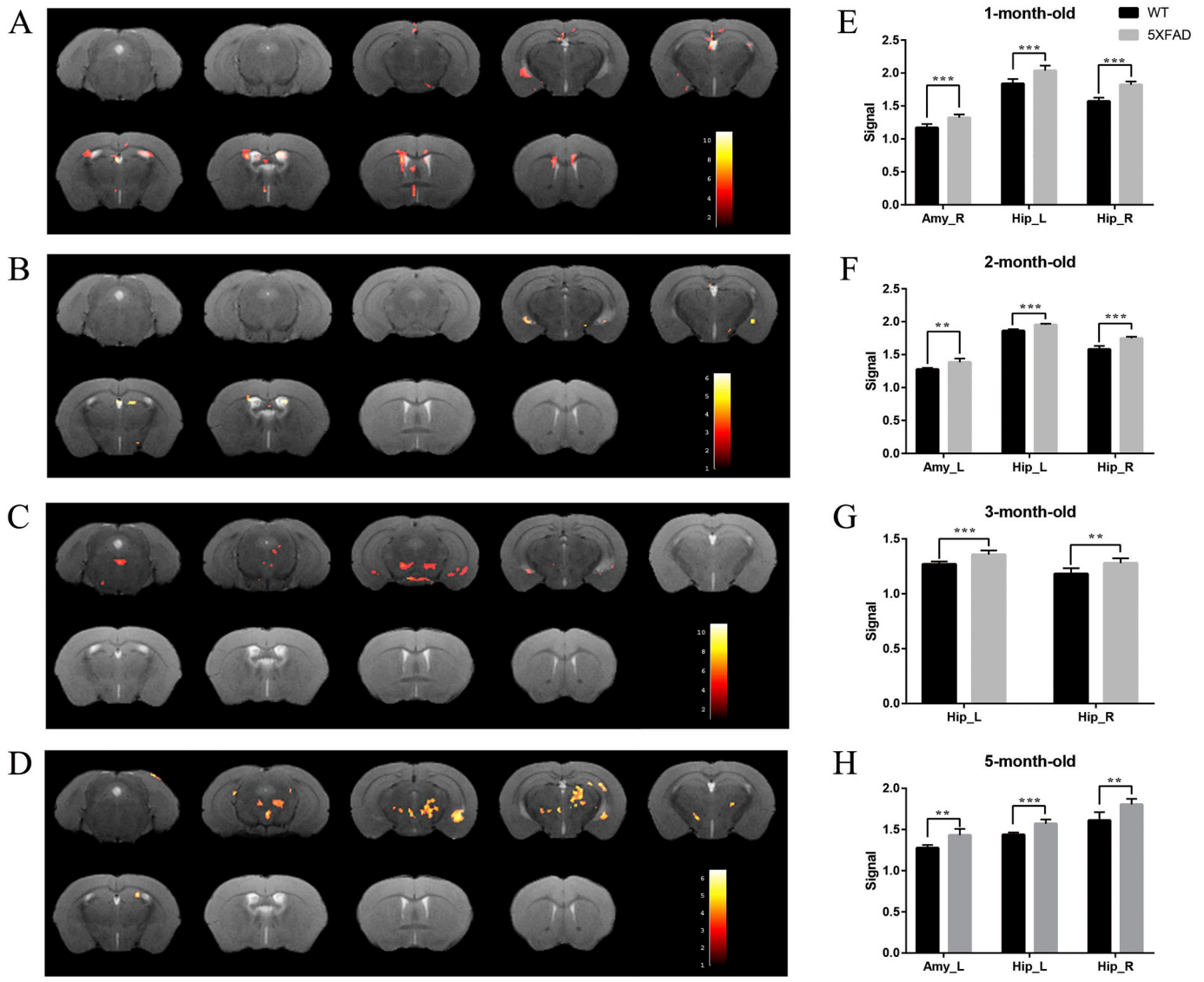

Fig. 7. Data analysis results of MEMRI images between 5XFAD and wild-type mice. (A–D) Voxel-wise analysis results. Comparing with the wild-type mice, the significant changes in 5XFAD mice at 1-, 2-, 3- and 5-month-old are superimposed on the IMT respectively. These significant voxels are shown in different artificial colors, while the anatomical structural image is presented in gray-scaled. The color bar stands for the T-value. (E–H) ROI-based quantitative analysis results. According to the voxel-wise analysis results, two significant ROIs, hippocampus and amygdala, are further analyzed quantitatively. The MEMRI signals of bilateral ROIs were analyzed between 5XFAD and wild-type mice at 1-, 2-, 3- and 5-month-old respectively. (**$P < 0.01$, ***$P < 0.001$, Amy: amygdala, Hip: hippocampus, R: right, L: left).

Our primary objective was to establish an effective and objective data analysis platform for MEMRI studies, in which a template set is prerequisite. The template image is always used as a standard reference in spatial normalization, so that it should be typical of the population's brain anatomy and has greater cross-subject validity [34]. In hence, a template image constructed from multi-subjects is preferable for group-level analysis. Therefore, in this study, a population IMT set was created for mouse brain using a validated template construction process [21,26], by iteratively registering and averaging. As shown in Fig. 4, the boundary of anatomical regions in IMT is smooth.

MEMRI images the distribution of Mn^{2+} with high sensitivity, which has been widely used for acquiring and analyzing data from the developing mouse brain [6,11]. Recently, a set of MEMRI templates of neonatal mouse brain between postnatal day 1 (P1) to P11 has been created [11], which has facilitated the early postnatal studies. In this study, an adult MEMRI template was created and application in late infancy researches, comprising stages of brain development between 1-month to 5-month. It was found that the spatial normalization of individual MEMRI images of developing mouse brain to the IMT space was satisfactory. Although the whole brain volume is always developing from 1-month-old to 5-month-old, the accuracy of spatial normalization is stabilized. As illustrated by the quantitative evaluation results (Table 2), the D_{coeff} between each normalized individuals in different developing stages and the IMT, comprising both the whole brain and sub-anatomical structures, is always higher than 95%, while both the FN and FP are always < 10%. Therefore, the IMT is an improvement and supplementary of previous studies.

In neuroimaging studies, an atlas image is also important, offering the stereotaxic sub-anatomical information, such as the Anatomical Automatic Labeling (AAL) atlas [35] and JHU white-matter tractography atlas [36] in human brain studies. Complementary to create an atlas image based on neuroimages [11,12], constructing a digital atlas image based on histological figures could identify subtle sub-anatomical structures. In this study, we created a digital mouse brain atlas image from the 2nd edition of Paxinos and Franklin atlas, in which 707 sub-anatomical structures in three dimensions were delineated (Fig. 5

Table 3
Brain regions with significant differences between 5XFAD and wild-type mice at 1-, 2-, 3-and 5-month-old via voxel-wise analysis ($P < 0.001$) and FDR correction for multiple comparisons at the cluster level.

	MAX_T	Clusters	X	Y	Z
1-month-old					
Amygdala right	5.1650	90	1.9899	5.0852	−1.8713
Caudate Putamen right	7.0056	230	0.9099	2.2840	0.9180
Cingulate Cortex left	6.1521	124	−0.6399	1.5268	0.0882
Habenula Nucleus right	7.6164	43	0.2337	2.1681	−0.9638
Hippocampus left	5.3922	34	−0.0585	1.7104	−1.6746
Hippocampus right	10.8485	163	0.3297	2.0392	−1.3184
Retrosplenial Cortex right	6.4005	65	0.2283	1.1400	−2.3879
Septal left	6.3594	46	−0.4431	2.1381	−0.0221
Septal right	5.7424	66	0.3321	2.5488	0.0992
Somatosensory Cortex right	5.4057	63	1.2921	1.4968	0.0842
Medial Prefrontal Cortex left	6.3840	163	−0.6387	1.7184	−0.1446
2-month-old					
Amygdala left	5.0261	32	−2.5557	4.2224	−1.8736
Hippocampus left	5.1215	39	−0.7335	1.9678	−1.0821
Hippocampus right	6.2314	53	0.1353	1.8427	−1.2029
3-month-old					
Hippocampus left	5.2216	196	−3.1335	4.4714	−2.9278
Ventral Tegmental Area right	7.9898	39	0.5391	4.6939	−3.4023
5-month-old					
Amygdala left	5.0334	28	−2.6529	4.1044	−2.1101
Hippocampus left	5.6186	264	−2.7483	4.2817	−2.5781
Hypothalamus left	5.4942	21	−0.9201	3.0246	−2.3621
Thalamus left	6.0514	251	−1.1151	2.7244	−2.2479
Visual Cortex left	6.4460	67	−2.3805	0.9425	−4.3847

and Appendix 0). The atlas image can mainly be used for assistance in localizing the voxel-wise analysis results, and automatically extracting sub-anatomical structures in ROI-wise analysis. Each sub-anatomical structure in this atlas image was assigned an integral value, which served not only as a database index but also as the voxel intensity. Therefore, a sub-anatomical structure could be easily located and extracted from the atlas by just reading the image intensity of each voxel. Furthermore, to preserve information concerning laterality, each sub-anatomical structure was assigned an odd/even integer for left/right. Moreover, these sub-anatomical structures could be merged optionally according to different researches.

The central piece of our efforts was to make the Paxinos and Franklin's mouse brain atlas image available in the coordinate space of IMT. In the view of our previous experience [21,22], the strategy of converting the atlas image into a pseudo MRI image was adopted and further improved. In this study, only gray matters of mouse brain were used in the image registration of the atlas and template. As shown in Fig. 3 and Fig. 6, the IMT has been co-registered with the mouse brain atlas excellently. Moreover, the method of manually tracing is always regarded as a golden standard, so that an expert was invited to trace out the CPu and Hip from the T2WI template image in IMT, blinded to the atlas image. Although the boundary of the substructures are not clear enough in MRI image, the volumetric and spatial correspondence measures between the atlas and template are also satisfactory. Therefore, by co-registering with the atlas image, the IMT is in the stereotaxic coordinate space of Paxinos and Franklin, and also has fine sub-anatomical structures delineations.

The usage and accuracy of a newly created template is always evaluated by applicating it in different studies. In this study, a group of developing 5XFAD mice at 1-, 2-, 3-, and 5-month-old were used to demonstrate the usage of IMT. By the voxel-wise analysis of MEMRI images, the locations of significant abnormal neuronal activity in 5XFAD mice at 1-, 2-, 3- and 5-month-old were found, which might reveal the progression of Alzheimer's disease. In this study, it was found the significantly increased signal in hippocampus of 5XFAD, which was consistent with the previous studies [6,37]. What's more, our study suggested some new discoveries which was not found in our previous study [6] by manual-trace ROI analysis. Interestingly, abnormal neuronal activity in many regions occurred in 5XFAD mice at 1-month-old, including amygdala, hippocampus, retrosplenial cortex, medial prefrontal cortex, cingulate cortex, caudate putamen, somatosensory cortex and septal. A previous study also reported alterations in similar regions in AD mice at 4-week-old [37]. The neuronal activity changes during the developmental stages might be associated with pre-pathogenesis in AD. In addition, the abnormal neuronal activity in hippocampus and amygdala was observed at early stage and sustained to 5-month-old in 5XFAD mice. In our previous study, it has found the impairment of spatial reference memory in 5XFAD since 1-month-old [6]. Both hippocampus and amygdala plays an important role in spatial learning and spatial reference memory [38–40]. We could speculate that the abnormal neuronal activity in hippocampus and amygdala might contribute to cognitive impairment in AD.

Moreover, the IMT is not only limited in MEMRI studies of mouse brain. It could be generalized in multi-modality MRI imaging data analyses, such as T2WI structural images, functional MRI (fMRI) images, and arterial spin labeling (ASL) images and so on. Conventionally, using the intensity-based registration method, multi-modality template images should be constructed for multi-modality images analyses, such as the T1-weighted template, the proton density (PD) template, and the positron emission tomography (PET) template in Montreal Neurological Institute (MNI) space for human brain studies [34]. Up to date, using the DARTEL algorithm in SPM, the spatial normalization is performed based on image segmentation, so that a set of TPM is enough. Our constructed TPM of mouse brain is compatible with the latest version of SPM. Based on this TPM, the DARTEL algorithm in SPM12 could be employed in spatial normalization of mouse brain images, which performs iteratively by segmenting the gray matter tissues from individual images and then registering them with the *GM* in TPM [24,25]. Therefore, based the TPM in IMT, multi-modality images of mouse brain could be spatially normalized and further analyzed. However, based on the DARTEL algorithm, the accuracy of spatial normalization is mainly depending on the segmentation of gray matters, which performs based on the individual image contrast and a prior location information, so that the segmentation would be failed when the image resolution is too low. Therefore, the limitation of the TPM in IMT is that it is not suitable for mouse brain images acquired on 3 T MRI or lower.

In addition, as the IMT comprises not only the intracranial tissues but also the extracranial parts, manually exclude extracranial tissues of individual images prior to spatial normalization is not required any more, which is time-consuming and labor-intensive.

5. Conclusion

In conclusion, we have constructed a stereotaxic template set of mouse brain named IMT with fine delineations of sub-anatomical structures in Paxinos and Franklin space, which is compatible with SPM. We believe that the IMT can properly support collaborations to answer important questions, such as the longitudinal trajectories of diseased brain functional developing, the consistency of functional connectivity across a population and so on. By providing an open IMT and software package for data analysis of mouse brain, the IMT will assist researchers pursuing the challenging diseases and further our understanding.

Acknowledgments

This work was supported by grants from the National Natural Science Foundation of China grant numbers [81471741, 81471728, 81501464, 81671770, 81701080].

Appendix A

Detailed information on some of the 707 structures included in the mouse brain atlas by Paxinos and Franklin and presented in Fig. 5B.

VOI ID	Structural name	Abbreviation	$Index_L$*	$Index_R$*
1	Retrosplenial granular cortex	RSG	1349	1350
2	Retrosplenial agranular cortex	RSA	1347	1348
3	Medial parietal association cortex	MPtA	1053	1054
4	Lateral parietal association cortex	LptA	885	886
5	Secondary visual cortex, lateral area	V2L	1593	1594
6	Primary somatosensory cortex, barrel field	S1BF	1363	1364
7	Secondary auditory cortex, ventral area	AuV	263	264
8	Temporal association cortex	TeA	1575	1576
9	Ectorhinal cortex	Ect	545	546
10	Perirhinal cortex	PRh	1273	1274
11	Piriform cortex	Pir	1173	1174
12	Posterolateral cortical amygdaloid nucleus (C2)	PLCo	1177	1178
13	Posteromedian cortical amygdaloid nucleus (C3)	PMCo	1187	1188
14	Amygdalohippocampal area, anterolateral part	AHiAL	155	156
15	Basomedial amygdaloid nucleus, posterior part	BMP	299	300
16	Basolateral amygdaloid nucleus, ventral part	BLV	295	296
17	Ventral endopiriform nucleus	VEn	1609	1610
18	Dorsal emdopiriform nucleus	DEn	461	462
19	Basolateral amygdaloid nucleus, posterior part	BLP	293	294
20	Basolateral amygdaloid nucleus, anterior part	BLA	291	292
21	Lateral amygdaloid nucleus, ventrolateral part	LaVL	783	784
22	Lateral amygdaloid nucleus, ventromediall part	LaVM	785	786
23	Lateral amygdaloid nucleus, dorsolateral part	LaDL	777	778
24	Caudate putamen (striatum)	CPu	407	408
25	Internal capsule	ic	667	668
26	Amygdalo striatal transition area	AStr	1721	1722
27	Central amygdaloid nucleus, lateral division	CeL	359	360
28	Bed nucleus of the stria terminalis, intra-amygdaloid division	BSTIA	309	310
29	Medial amygdaloid nucleus, posterodorsal part	MePD	961	962
30	Medial amygdaloid nucleus, posterobentral part	MePV	963	964
31	Lateral ventricle	LV	905	906
32	Fimbria of the hippocampus	fi	575	576
33	Optic tract	opt	1093	1094
34	Supraoptic decussation	sox	1503	1504
35	Cerebral peduncle, basal part	cp	403	404
36	Reticular thalamic nucleus	Rt	1351	1352
37	External medullary lamina	eml	553	554
38	Medial lemniscus	ml	989	990
39	Subthalamic nucleus	STh	1537	1538
40	Zona incerta, ventral part	ZIV	1713	1714
41	Zona incerta, dorsal part	ZID	1711	1712
42	Nigrostriatal bundle	ns	1079	1080
43	Magnocellular nucleus of the lateral hypothalamus	MCLH	921	922
44	Lateral hypothalamic area	LH	805	806
45	Mammillothalamic tract	mt	1063	1064
46	A11 dopamine cells	A11	115	116
47	Posterior hypothalamic area	PH	1167	1168
48	Dorsomedial hypothalamic nucleus, dorsal part	DMD	487	488
49	Dorsomedial hypothalamic nucleus, compact part	DMC	485	486
50	Dorsomedial hypothalamic nucleus, ventral part	DMV	497	498
51	Perifornical nucleus	PeF	1159	1160
52	fornix	f	569	570
53	Terete hypothalamic nucleus	Te	1573	1574
54	Medial tuberal nucleus	MTu	1067	1068
55	Ventromedial hypothalamic nucleus, ventrolateral part	VMHVL	1669	1670
56	Ventromedial hypothalamic nucleus, central part	VMHC	1665	1666
57	Ventromedial hypothalamic nucleus, dorsomedial part	VMHDM	1667	1668
58	Arcuate hypothalamic nucleus, dorsal part	ArcD	217	218
59	Arcuate hypothalamic nucleus, lateral part	ArcL	219	220
60	Median eminence	ME	941	942
61	3rd ventricle	3V	71	72
62	Periventricular hypothalamic nucleus	Pe	1157	1158
63	Ventromedial thalamic nucleus	VM	1661	1662
64	Superior cerebellar peduncle (brachium conjunctivum)	scp	1289	1290
65	Ventral posterolateral thalamic nucleus	VPL	1681	1682
66	Ventral posteromedial thalamic nucleus	VPM	1683	1684
67	Posterior thalamic nuclear group	Po	1209	1210
68	Dorsal lateral geniculate nucleus	DLG	473	474
69	Ventral lateral geniculate nucleus	VLG	1617	1618
70	Lateral posterior thalamic nucleus, laterorostral part	LPLR	877	878
71	Lateral posterior thalamic nucleus, mediocaudal part	LPMR	881	882
72	Centrolateral thalamic nucleus	CL	391	392

73	Paracentral thalamic nucleus	PC	1137	1138
74	Oval paracentral thalamic nucleus	OPC	1089	1090
75	Central medial thalamic nucleus	CM	397	398
76	Mediodorsal thalamic nucleus, medial part	MDM	937	938
77	Mediodorsal thalamic nucleus, central part	MDC	931	932
78	Mediodorsal thalamic nucleus, lateral part	MDL	935	936
79	Fasciculus retroflexus	fr	583	584
80	Lateral habenular nucleus, lateral part	LHbL	809	810
81	Lateral habenular nucleus, medial part	LHbM	811	812
82	Habenular commissure	hbc	619	620
83	Medial habenular nucleus	MHb	977	978
84	Dorsal 3rd ventricle	D3V	453	454
85	Paraventricular thalamic nucleus	PV	1289	1290
86	Superior cerebellar peduncle (brachium conjunctivum)	scp	1403	1404
87	Intermediodorsal thalamic nucleus	IMD	691	692
88	Posteromedian thalamic nucleus	PoMn	1213	1214
89	cingulum	cg	369	370
90	Corpus callosum	cc	353	354
91	Alveus of the hippocampus	alv	173	174
92	Oriens layer of the hippocampus	Or	1095	1096
93	Pyramidal cell layer of the hippocampus	Py	1297	1298
94	Stratum	Rad	1305	1306
95	Stratum lucidum, hippocampus	SLu	1461	1462
96	Lacunosum molecular layer of the hippocampus	LMol	819	820
97	Molecular layer of the dentate gyrus	Mol	1005	1006
98	Granular layer of the dentate gyrus	GrDG	613	614
99	Polymorph layer of the dentate gyrus	PoDG	1211	1212
100	Dentate gyrus	DG	465	466
101	Dorsal fornix	df	463	464
102	Fasciola cinereum	FC	571	572

References

[1] Fu HJ, Rodriguez GA, Herman M, Emrani S, Nahmani E, Barrett G, et al. Tau pathology induces excitatory neuron loss, grid cell dysfunction, and spatial memory deficits reminiscent of early Alzheimer's disease. Neuron 2017;93(3). (533-+).

[2] Silva AC, Lee JH, Aoki L, Koretsky AR. Manganese-enhanced magnetic resonance imaging (MEMRI): methodological and practical considerations. NMR Biomed 2004;17(8):532–43.

[3] Lutkenhoff E, Karlsgodt KH, Gutman B, Stein JL, Thompson PM, Cannon TD, et al. Structural and functional neuroimaging phenotypes in dysbindin mutant mice. Neuroimage 2012;62(1):120–9.

[4] Wang YM, Cella M, Mallinson K, Ulrich JD, Young KL, Robinette ML, et al. TREM2 lipid sensing sustains the microglial response in an Alzheimer's disease model. Cell 2015;160(6):1061–71.

[5] Criscuolo C, Cerri E, Fabiani C, Capsoni S, Cattaneo A, Domenici L. The retina as a window to early dysfunctions of Alzheimer's disease following studies with a 5xFAD mouse model. Neurobiol Aging 2018;67:181–8.

[6] Tang X, Wu D, Gu LH, Nie BB, Qi XY, Wang YJ, et al. Spatial learning and memory impairments are associated with increased neuronal activity in 5XFAD mouse as measured by manganese-enhanced magnetic resonance imaging. Oncotarget 2016;7(36):57556–70.

[7] Sawiak SJ, Wood NI, Williams GB, Morton AJ, Carpenter TA. Voxel-based morphometry with templates and validation in a mouse model of Huntington's disease. Magn Reson Imaging 2013;31(9):1522–31.

[8] Ullmann JFP, Watson C, Janke AL, Kurniawan ND, Reutens DC. A segmentation protocol and MRI atlas of the C57BL/6J mouse neocortex. Neuroimage 2013;78:196–203.

[9] Ullmann JFP, Watson C, Janke AL, Kurniawan ND, Paxinos G, Reutens DC. An MRI atlas of the mouse basal ganglia. Brain Struct Funct 2014;219(4):1343–53.

[10] Hikishima K, Komaki Y, Seki F, Ohnishi Y, Okano HJ, Okano H. In vivo microscopic voxel-based morphometry with a brain template to characterize strain-specific structures in the mouse brain. Sci Rep 2017;7.

[11] Szulc KU, Lerch JP, Nieman BJ, Bartelle BB, Friedel M, Suero-Abreu GA, et al. 4D MEMRI atlas of neonatal FVB/N mouse brain development. Neuroimage 2015;118:49–62.

[12] Chuang N, Mori S, Yamamoto A, Jiang H, Ye X, Xu X, et al. An MRI-based atlas and database of the developing mouse brain. Neuroimage 2011;54(1):80–9.

[13] Mccarthy M. Allen Brain Atlas maps 21000 genes of the mouse brain. Lancet Neurol 2006;5(11):907–8.

[14] Dang C, Sodt A, Lau C, Youngstrom B, Ng L, Kuan L, et al. The allen brain atlas: delivering neuroscience to the web on a genome wide scale. Data Integration in the Life Sciences, Proceedings. 4544. 2007. (17-+).

[15] Paxinos G, Franklin KBJ. The Mouse Brain: In Stereotaxic Coordinates. San Diego: Academic Press; 2001.

[16] Ashburner J. SPM: a history. Neuroimage 2012;62(2):791–800.

[17] Oakley H, Cole SL, Logan S, Maus E, Shao P, Craft J, et al. Intraneuronal beta-amyloid aggregates, neurodegeneration, and neuron loss in transgenic mice with five familial Alzheimer's disease mutations: potential factors in amyloid plaque formation. J Neurosci 2006;26(40):10129–40.

[18] Tustison NJ, Avants BB, Cook PA, Zheng Y, Egan A, Yushkevich PA, et al. N4ITK: improved N3 bias correction. IEEE Trans Med Imaging 2010;29(6):1310–20.

[19] Friston KJ, Ashburner J, Frith CD, Poline JB, Heather JD, Frackowiak RSJ. Spatial registration and normalization of images. Hum Brain Mapp 1995;3(3):165–89.

[20] Zhilkin P, Alexander ME. Affine registration: a comparison of several programs. Magn Reson Imaging 2004;22(1):55–66.

[21] Nie B, Chen KW, Zhao SJ, Liu JH, Gu XC, Yao QL, et al. A rat brain MRI template with digital stereotaxic atlas of fine anatomical delineations in paxinos space and its automated application in voxel-wise analysis. Hum Brain Mapp 2013;34(6):1306–18.

[22] Nie BB, Liu H, Chen KW, Jiang XF, Shan BC. A statistical parametric mapping toolbox used for voxel-wise analysis of FDG-PET images of rat brain. Plos One 2014;9(9).

[23] Ashburner J. A fast diffeomorphic image registration algorithm. Neuroimage 2007;38(1):95–113.

[24] Ashburner J, Friston KJ. Unified segmentation. Neuroimage 2005;26(3):839–51.

[25] Klein A, Andersson J, Ardekani BA, Ashburner J, Avants B, Chiang MC, et al. Evaluation of 14 nonlinear deformation algorithms applied to human brain MRI registration. Neuroimage 2009;46(3):786–802.

[26] Liang SX, Wu S, Huang Q, Duan SF, Liu H, Li YX, et al. Rat brain digital stereotaxic white matter atlas with fine tract delineation in Paxinos space and its automated applications in DTI data analysis. Magn Reson Imaging 2017;43:122–8.

[27] Gutierrez DF, Zaidi H. Automated analysis of small animal PET studies through deformable registration to an atlas. Eur J Nucl Med Mol Imaging 2012;39(11):1807–20.

[28] Van Horn JD, Ellmore TM, Esposito G, Berman KF. Mapping voxel-based statistical power on parametric images. Neuroimage 1998;7(2):97–107.

[29] Nie B, Liang SX, Jiang XF, Duan SF, Huang Q, Zhang TH, et al. An automatic method for generating an unbiased intensity normalizing factor in positron emission tomography image analysis after stroke. Neurosci Bull 2018;34(5):833–41.

[30] Chupin M, Mukuna-Bantumbakulu AR, Hasboun D, Bardinet E, Baillet S, Kinkingnehun S, et al. Anatomically constrained region deformation for the automated segmentation of the hippocampus and the amygdala: method and validation on controls and patients with Alzheimer's disease. Neuroimage 2007;34(3):996–1019.

[31] Murugavel M, Sullivan JM. Automatic cropping of MRI rat brain volumes using pulse coupled neural networks. Neuroimage 2009;45(3):845–54.

[32] Rodionov R, Chupin M, Williams E, Hammers A, Kesavadas C, Lemieux L. Evaluation of atlas-based segmentation of hippocampi in healthy humans. Magn Reson Imaging 2009;27(8):1104–9.

[33] Aragon-Sanchez J, Quintana-Marrero Y, Aragon-Hernandez C, Hernandez-Herero MJ. ImageJ: a free, easy, and reliable method to measure leg ulcers using digital pictures. Int J Low Extrem Wounds 2017;16(4):269–73.

[34] Mazziotta JC, Toga AW, Evans A, Fox P, Lancaster J. A probabilistic atlas of the human brain - theory and rationale for its development. Neuroimage 1995;2(2):89–101.

[35] Tzourio-Mazoyer N, Landeau B, Papathanassiou D, Crivello F, Etard O, Delcroix N, et al. Automated anatomical labeling of activations in SPM using a macroscopic anatomical parcellation of the MNI MRI single-subject brain. Neuroimage 2002;15(1):273–89.
[36] Mori S, Oishi K, Jiang HY, Jiang L, Li X, Akhter K, et al. Stereotaxic white matter atlas based on diffusion tensor imaging in an ICBM template. Neuroimage 2008;40(2):570–82.
[37] Allemang-Grand R, Scholz J, Ellegood J, Cahill LS, Laliberte C, Fraser PE, et al. Altered brain development in an early-onset murine model of Alzheimer's disease. Neurobiol Aging 2015;36(2):638–47.
[38] Rumpel S, Ledoux J, Zador A, Malinow R. Postsynaptic receptor trafficking underlying a form of associative learning. Science 2005;308(5718):83–8.
[39] Liang SX, Huang J, Liu WL, Jin H, Li L, Zhang XF, et al. Magnetic resonance spectroscopy analysis of neurochemical changes in the atrophic hippocampus of APP/PS1 transgenic mice. Behav Brain Res 2017;335:26–31.
[40] Danjo T, Toyoizumi T, Fujisawa S. Spatial representations of self and other in the hippocampus. Science 2018;359(6372):213–8.